Large area deposition of Pb(Zr,Ti)O$_3$ thin films for piezoelectric MEMS devices

**Gunnar Suchaneck · Vinay S. Vidyarthi ·
Marianne Reibold · Alexander Deyneka ·
Lubomir Jastrabik · Gerald Gerlach ·
Johannes Hartung**

Abstract Pb(Zr,Ti)O$_3$ (PZT) thin films deposited on insulating ZrO$_2$ buffered silicon wafer are intended to be employed for in-plane polarized piezoelectric MEMS devices. Multi-target reactive sputtering system for large area deposition of in-situ crystallized PZT thin films and the ZrO$_2$ buffer layer has been employed. The interface analysis of multilayer structures by high resolution transmission microscope, X-ray diffraction, optical refraction, and absorption spectra studies has been presented. At a substrate temperature of 520°C and excess lead deposition condition, the formation of a PZT superstructure has been revealed. The substrate temperature of 580°C leads to the crystallization of PZT directly into a single phase perovskite crystal structure. A pronounced Urbach behavior in our PZT thin films has been observed by optical absorption studies. The surface roughness of PZT films deposited on a ZrO$_2$ buffer layer is much higher than that on conducting platinized silicon wafer.

G. Suchaneck (✉) · V. S. Vidyarthi · G. Gerlach
Institut für Festkörperelektronik, Technische Universität Dresden,
Helmholtzstrasse 18,
01062 Dresden, Germany
e-mail: Gunnar.Suchaneck@tu-dresden.de

M. Reibold
Institute of Structure Physics, Technische Universität Dresden,
Zellescher Weg 16,
01062 Dresden, Germany

A. Deyneka · L. Jastrabik
Institute of Physics, AS CR,
18221 Prague 8, Czech Republic

J. Hartung
Von Ardenne Anlagentechnik GmbH,
Plattleite 19/29,
01324 Dresden, Germany

1 Introduction

Using interdigital electrodes for device poling, ferroelectric polarization is aligned in the plane of ferroelectric film. In-plane polarized PZT enables the longitudinal d_{33} mode to be exploited in transducer applications. In this case, film thickness and electrode spacing of the transducers become independent of each other, giving degrees of freedom in adjusting the capacitance of the device to be matched with the peripheral circuit or to be minimized in order to enhance sensor voltage sensitivity. Additional degrees of freedom become available also in choosing buffer or seeding layers as well as substrates for the growth of ferroelectric films. Moreover, the sensor performance will not be affected by interlayer defects and stray capacitance in the normal direction of the film [1]. In-plane polarized ferroelectric thin films on ZrO$_2$ buffered silicon substrates, which are required for high-sensitivity devices, were previously deposited by chemical solution deposition (CSD) and a subsequent high temperature annealing [2–4]. In order to improve film quality, the ZrO$_2$ buffer layer was manufactured also by pulsed laser deposition [5]. Recently, we have reported a multi-target reactive sputter deposition of a ZrO$_2$ barrier layer and a PZT thin film suitable for piezoelectric applications in one process run onto 150 mm oxidized silicon wafers [6, 7]. However, little attention has been paid yet to the investigation of the interfaces between the substrate, the ZrO$_2$ buffer layer and the PZT thin film.

In this work, the interfaces of in-situ crystallized PZT thin films deposited by industrial-scale equipment onto standard oxidized silicon wafers comprising a buffer layer have been

Table 1 Deposition conditions of ZrO_2 and PZT films.

	ZrO_2	PZT
Target diameter (mm)	200	200
Target-substrate distance (mm)	65	65
RF power at Pb (W)		450
DC pulsed power at Zr (W)	800	800
DC pulsed power at Ti (W)		2000
Total gas Pressure (mbar)	$6 \cdot 10^{-3}$	$6 \cdot 10^{-3}$
Argon flow (sccm)	75	75
Oxygen flow (sccm)	10	10 (Pb, Zr) 0–10
		(Ti, PEM-controlled)
Substrate temperature (°C)	550	520–580

investigated by high resolution transmission electron microscopy (HRTEM). The PZT films can be polarized in-plane by biasing an interdigital electrode structure. These are suitable for piezoelectric MEMS applications.

2 Experimental

Multi-target reactive sputter deposition was performed in a LS730S sputtering system (Von Ardenne Anlagentechnik GmbH, Dresden). The computer controlled system is equipped with a process chamber and a load-lock, both evacuated by turbomolecular pumps. The process chamber consists of four 8" metal targets, two stationary radiation heaters and a wafer carousel holding four 150 mm silicon wafers. Chamber pressure is controlled via a butterfly valve. To prevent arcing during reactive sputtering, units for pulsed DC (30 kHz, duty cycle ~90%) and arc

suppression (Advanced Energy Pinnacle) are connected between the power supplies and the Ti and Zr targets. The Pb target is directly connected with the RF (13.56 MHz) generator. Additional oxygen gas channels, which are controlled by piezoelectric valves, are introduced near the target surfaces. The gas flow of one channel is controlled by a closed-loop feed-back circuit of the plasma emission monitor (PEM).

The 150 mm silicon wafers were covered with a 500 nm thermally grown SiO_2 layer. Both ZrO_2 (thickness 220 nm) and then PZT films (thickness 350 to 2,000 nm) were sputtered in an argon/oxygen mixture at a total pressure of $6 \cdot 10^{-3}$ mbar. The substrate temperature was kept at about 550°C for ZrO_2 and at 480 to 580°C for PZT. Argon flow was fixed at 75 standard cubic centimeters per minute (sccm). ZrO_2 films were sputtered on the SiO_2/Si substrates at 800 W to the Zr target. The sputtering process was done near the transition region. The oxygen flow was controlled dynamically by the PEM unit using a Zr spectral line emission ($\lambda=360$ nm) of the plasma as a set point for the piezoelectric valve. For PZT deposition, the oxygen supply to the Pb and Zr targets were fixed at 10 sccm. The admission of oxygen to the Ti target was controlled by PEM via a Ti spectral line ($\lambda=453$ nm) intensity [7]. At a substrate temperature of 580°C, the PZT films grew in-situ in the ferroelectric perovskite phase, i.e., no thermal treatment after deposition was needed. At lower substrate temperatures, the films are not fully crystallized into perovskite phase. The ZrO_2 and PZT deposition conditions are summarized in Table 1.

X-ray diffraction (XRD) patterns were recorded by a Phillips X-Pert diffractometer (Co − K_α) in the θ–2θ mode.

**Fig. 1** XRD pattern of a ZrO_2/SiO_2/Si structure; *m* monoclinic ZrO_2, *t* tetragonal ZrO_2)
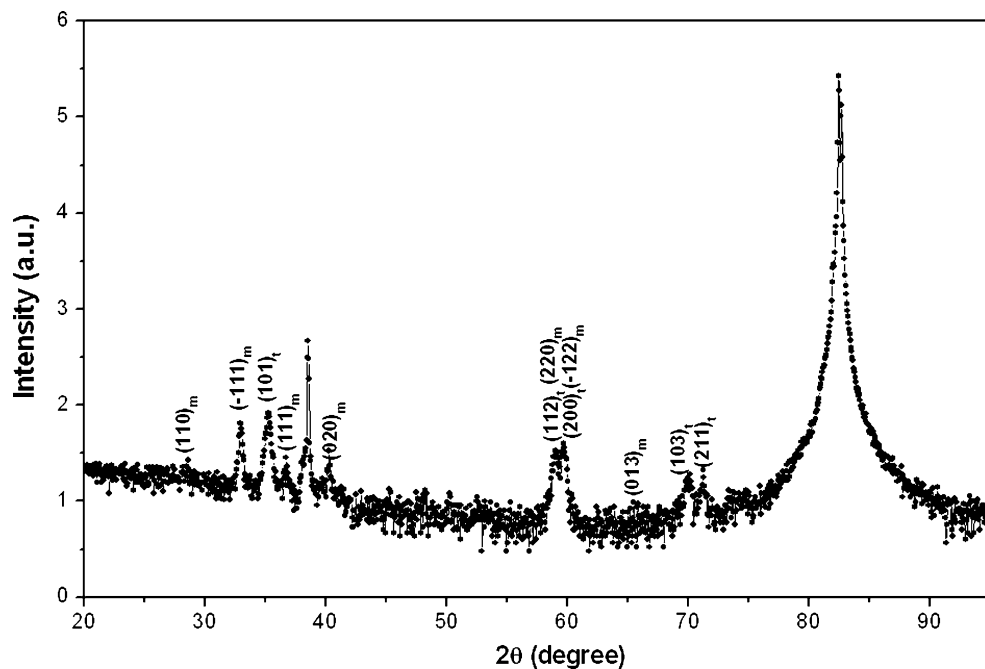
The peak positions were compared with the JCPDS database.

HRTEM investigation was performed at the Triebenberg Laboratory (http://www.triebenberg.de), Institute of Structure Physics, by means of a Phillips CM30 Transmission Electron Microscope operated at 300 kV. The original sample was cut into two pieces, glued (with an epoxy resin) in such way that the thin films of both pieces are disposed face to face, and sawed into thin slices. The resulting sample is thereafter thinned first mechanically by grinding and polishing followed by argon ion milling till electron transparency.

Refractive and absorption index spectra and film anisotropy were calculated from main ellipsometric angles Δ and Ψ measured with a J. A. Woollam spectroscopic ellipsometer. The ellipsometric data were analyzed with the software package WVASE32. For calculation of PZT absorption, a simple (substrate)/(one layer) model was
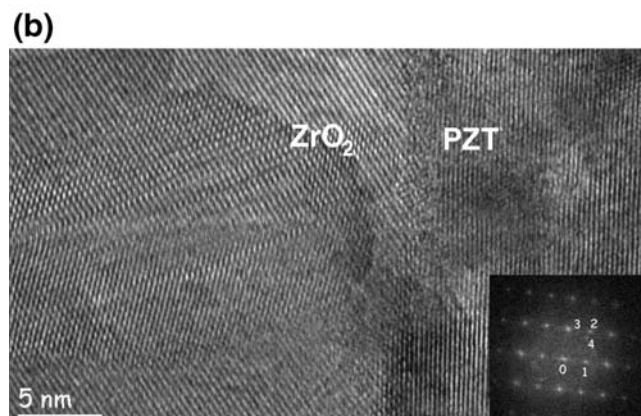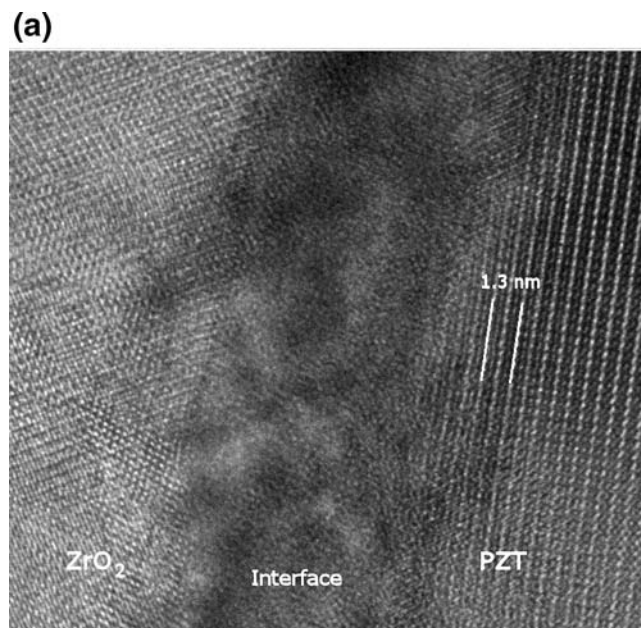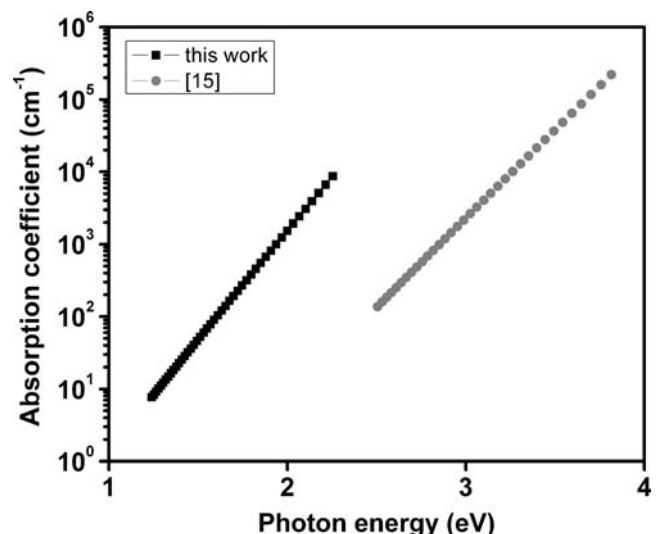
Fig. 3 Optical absorption coefficients of a $Pb(Pb_{0.31}Zr_{0.28}Ti_{0.41})O_3$ film deposited onto a ZrO_2 buffer layer (this work) and a $Pb(Pb_{0.10}Zr_{0.21}Ti_{0.69})O_3$ film deposited onto a platinized silicon wafer [15]

used. Therefore, all optical constants obtained are "effective" ones neglecting surface and interface effects [8]. The films were considered isotropic in our calculation. Arguments for this approximations and a detailed information about calculations are presented in [9].

3 Results and discussion

Figure 1 shows an X-ray diffractogram of the ZrO_2 buffer layer. The peaks at 35.268°, 41.232°, 59.732°, and 71.302° were assigned to tetragonal ZrO_2 with lattice parameters of $a=0.3592$ nm and $c=0.5183$ nm (JCPDS number 79-1771) while that at 28.458°, 32.327°, 36.694°, 40.152°, 58.89°, 59.434°, and 65.254° correspond to the monoclinic ZrO_2 phase with lattice constants of $a=0.5150$ nm $b=0.5211$ nm, $c=0.5317$ nm, and $\beta=99.230°$ (JCPDS number 37-1484).

For PZT thin films deposited at a substrate temperature of 520°C, an amorphous interface layer occurs as shown in Fig. 2(a). This figure further illustrates the appearance of a PZT superstructure. It was assigned to the orthorhombic space group *I2mm*. This indicates the appearance of a Ruddlesden-Popper phase $Pb_2(Zr,Ti)O_4$. Previously, a similar Pb_2TiO_4 structure was found to be stabilized by V_2O_5 in a PbO-V_2O_5-TiO_2 system [10]. Pb_2TiO_4 was obtained also at the surface of $PbTiO_3$ single crystals [11]. Moreover, the possibility of Ruddlesden-Popper phase formation in $PbTiO_3$ was predicted recently by first principle density function theory calculations [12]. In PZT thin films $Pb_2(Zr,Ti)O_4$ was observed for the first time in [7]. The lattice constants derived from the XRD pattern were $a \approx 0.39$ nm, $b \approx 0.375$ nm, and $c \approx 1.3$ nm. Thus, the lattice parameter c is in good agreement with the lattice plane spacing obtained

Fig. 2 HRTEM micrographs of ZrO_2/PZT interface for a PZT deposition temperature of 520°C (**a**) and 580°C (**b**)

in the HRTEM image. Obviously, lead-enriched interface layers near the ZrO_2/PZT interface favor $Pb_2(Zr,Ti)O_4$ nucleation. ZrO_2 buffer layers are known to act as lead diffusion barrier [13, 14]. Consequently, lead diffusion was confined to the PZT/ZrO_2 interface resulting in a lead-enriched amorphous interface layer at 520°C as proofed by GD-OES composition profiling [7].

Increasing the PZT deposition temperature beyond 580°C, the amorphous interface layer disappears but some lattice strain still remains [Fig. 2(b)]. Electron diffraction pattern of the PZT region in the transmission electron microscope were assigned to 1—(100), 2—(111), 3—(101) and 4—(110) in good agreement with previous XRD data [7]. The corresponding lattice spacings were 0.4055, 0.2327, 0.2896, and 0.2849 nm, respectively.

Figure 3 compares the effective absorption coefficient of a $Pb(Pb_{0.31}Zr_{0.28}Ti_{0.41})O_3$ film deposited at 580°C onto a ZrO_2 buffer layer with the absorption behavior of an Pb $(Pb_{0.10}Zr_{0.21}Ti_{0.69})O_3$ film deposited onto a platinized silicon wafer [15]. Both samples show a pronounced Urbach behavior. Recently, we have shown that the increase of the Urbach tails of smooth films is caused by an increasing disorder introduced by tetravalent lead [15]. Here, we have to take into account also the different surface roughness. Therefore, the higher effective absorption of PZT films deposited onto a ZrO_2 buffer layer reflects the contribution of surface scattering. The r.m.s. surface roughness in this case amounts to about 45 nm, compared to 4...5 nm for the film on the platinized silicon substrate. Thereby, the surface roughness is mainly determined by the roughness of the substrate. Neither XRD pattern nor HRTEM images give evidence of secondary phase formation at the PZT/ZrO_2 interface in films deposited at 580°C. Therefore, excess PbO can be ruled out in our case as an origin of increased absorption at short wavelengths as discussed in [16].

4 Conclusions

The deposition conditions of multi-target reactive sputtering of PZT thin films onto oxidized 150 mm silicon wafers comprising a ZrO_2 buffer layer were investigated. A substrate temperature of 580°C is required to avoid the formation of an amorphous interface layer. The deposition technology described here can be easily scaled-up for larger silicon wafers and is compatible with standard semiconductor technology. After conditioning of a freshly cleaned reactor, it provides a reliable and reproducible device fabrication methodology which can be exploited up to onset of blistering. The latter depends on cleaning treatment of the inner parts of the reactor and on the use of special adhesion coatings improving anti-blistering properties.

References

1. S.J. Gross, S. Tadigadapa, T.N. Jackson, S. Trolier-McKinstry, Q.Q. Zhang, Appl. Phys. Lett. **83**, 174 (2003).
2. B. Xu, Y. Ye, L.E. Cross, Appl. Phys. Lett. **74**, 3549 (1999).
3. Z.T. Song, N. Chong, H.L.W. Chan, C.L. Choy, Appl. Phys. Lett. **79**, 668 (2001).
4. Q. Zhou, Q. Zhang, B. Xu, S. Trolier-Mc-Kinstry, J. Am. Ceram. Soc. **85**, 1997 (2002).
5. Z.T. Song, H.L.W. Chan, C.L. Choy, C.L. Lin, Microelectron. Eng. **66**, 887 (2003).
6. G. Suchaneck, W.-M. Lin, V. S. Vidyarthi, G. Gerlach, J. Hartung J. Europ. Ceram. Soc. **27**, 3789 (2007).
7. V.S. Vidyarthi, W.-M. Lin, G. Suchaneck, G. Gerlach, C. Thiele, V. Hoffmann, Thin Solid Films **515**, 3547 (2007).
8. A. Deineka, M. Glinchuk, L. Jastrabik, G. Suchaneck, T. Sandner, G. Gerlach, Ferroelectrics **258**, 271 (2001).
9. A. Deineka, M. Glinchuk, L. Jastrabik, G. Suchaneck, G. Gerlach, Phys. Stat. Sol. (a) **175**, 443 (1999).
10. I.N. Belyaev, A.K. Nesterova, Zh. Obsh. Khim. **22**, 396 (1952).
11. K. Szot, M. Pawelczyk, J. Herion, Ch. Freiburg, J. Albers, R. Waser, J. Hullinger, J. Kwapulinski, J. Dec, Appl. Phys. A **62**, 335 (1996).
12. C.J. Fennie, K.M. Rabe, Phys. Rev. B **71**, 100102R (2005).
13. T. Maeder, L. Sagalowicz, P. Muralt, Jpn. J. Appl. Phys. **37**, 2007, (1998).
14. Y. Jeon, J. Chung, K. No, J. Electroceram. **4**, 195 (2000).
15. G. Suchaneck, Wen-Mei Lin, G. Gerlach, A. Deyneka, L. Jastrabik, Integrated Ferroelectrics **80**, 189 (2006).
16. S. Trolier-McKinstry, H. Hu, S. B. Krupanidhi, P. Chindaudom, K. Vedam, R. E. Newnham, Thin Solid Films **230**, 15 (1993).